Japan J. Indust. Appl. Math., 22 (2005), 57–75 Area ⟨1⟩

Rigorous Numerics for Localized Patterns to the Quintic Swift-Hohenberg Equation

Yasuaki HIRAOKA and Toshiyuki OGAWA

Department of Mathematical Science,
Graduate School of Engineering Science, Osaka University,
Machikaneyama 1-3, Toyonaka, Osaka 560-8531, Japan

Received May 22, 2004

Localized patterns of the quintic Swift-Hohenberg equation are studied by bifurcation analysis and rigorous numerics. First of all, fundamental bifurcation structures around the trivial solution are investigated by a weak nonlinear analysis based on the center manifold theory. Then bifurcation structures with large amplitude are studied on Galerkin approximated dynamical systems, and a relationship between snaky branch structures of saddle-node bifurcations and localized patterns is discussed. Finally, a topological numerical verification technique proves the existence of several localized patterns as an original infinite dimensional problem, which are beyond the local analysis.

Key words: quintic Swift-Hohenberg equation, localized patterns, snaky bifurcation structure, rigorous numerics, Conley index

1. Introduction

In this paper, we study the following quintic Swift-Hohenberg equation:

$$u_t = \left\{ \nu - \left(1 + \frac{\partial^2}{\partial x^2} \right)^2 \right\} u + \mu u^3 - u^5. \tag{1}$$

In particular, our main interest is devoted to stationary localized patterns of this equation. Sakaguchi and Brand [14] observe by computer simulations that the quintic Swift-Hohenberg equation may have many types of stable localized stationary solutions in suitable parameter regions. Furthermore, they heuristically explain the relation between the existence of the stable localized patterns and the coexistence of stable uniform solutions and stable spatially periodic(roll) solutions, which is realized in the subcritical region ($\nu < 0$).

From the viewpoint of the stationary problems, *i.e.* the fourth order ordinary differential equations, there has been several studies for localized patterns by different approaches in recent years. Budd et al. [1] study post-buckling states of the classical elastic strut problem by the asymptotic expansion technique. They derive an amplitude equation from the original fourth order differential equation and show that there exist homoclinic orbits to the origin corresponding to the localized solutions. Moreover, heteroclinic connections between uniform solutions and periodic solutions are also studied by their analysis. The paper [17] also treats this problem by the combination of asymptotic and numerical methods, and it succeeds in capturing double-hump solutions and these snaky bifurcation structures.

The Hamiltonian-Hopf bifurcation (or degenerate reversible 1-1 resonance bifurcation [7]) is one of the other key issues to investigate localized solutions of the fourth order ordinary differential equations [5, 18]. In these papers they also found the similar phenomena, *i.e.* localized solutions and their snaky bifurcation structures, by the normal form analysis and numerical approaches.

Although the approaches are different from each other, these works described above are summarized as follows. They first analytically prove the existence of localized homoclinic solutions around the bifurcation point. Then the snaky bifurcation structures are derived by exploiting the numerical continuation technique. All these works are remarkably important not only to study localized solutions but also to discover the fascinating snaky bifurcation structures. However, it seems to be difficult to prove the existence of the snaky branches and to clarify the relationship between the localized solutions and the snaky bifurcation structures by the theoretical approaches. It is no wonder of this situation, since asymptotic analysis and normal form method essentially treat small amplitude phenomena. On the other hand, the stationary solutions on the snaky branches derived by the numerical branch continuations have essentially large amplitude. One of the main purposes of this paper is to directly investigate the stationary solutions on the snaky branches by a rigorous numerical technique.

Our strategy is to study the problem under the periodic boundary condition with reasonably large period by a weak nonlinear analysis and a topological rigorous numerical technique. In Section 2.1, a center manifold reduction to the quintic Swift-Hohenberg equation is performed in order to study local bifurcation structures. From this analysis, it is explained that pure mode branches bifurcate from the trivial solution as a subcritical pitchfork type at a simple critical point. On the other hand, at parameter values close to double critical points, we observe that stable mixed mode branches appear and lose their stability by a subcritical pitchfork bifurcation. Moreover, we conclude that imperfections of this subcritical pitchfork bifurcation occur and "Z-shaped" mixed mode branches are observed in generic cases.

Next, in order to proceed our studies to the regions away from bifurcation points, a numerical branch continuation technique [8] is adopted to Galerkin approximated quintic Swift-Hohenberg equation in Section 2.2. It is observed that snaky structures of saddle-node bifurcations arise along the secondary bifurcation branches (*i.e.* mixed mode branches) and localized patterns correspond to the equilibria on lower layers of these snaky structures (see Figure 7). We expect that these periodic stationary solutions converge to the homoclinic stationary solutions. In fact, as we discuss in Section 4, similar snaky branches appear by taking larger periods and corresponding solutions seem to converge to the homoclinic stationary solutions. We also discuss how aftereffects of these successive saddle-node bifurcations affect invading dynamics observed by computer simulations.

It is natural to consider whether these localized patterns observed at lower layers of snaky branches in the finitely approximated problem really exist in the original quintic Swift-Hohenberg equation. To answer this naive question, we verify

the existence of these patterns by using a topological numerical verification method. This method is first developed in [19] and a key tool for this method is the Conley index, topological quantities defined on invariant set for dynamical systems (see Section 3.1 for the definition). We here point out that one of the advantages to adopt the topological verification method is that not only proving the existence of equilibria but also we may detect connecting orbits between verified equilibria by using the Conley index theory. In fact, this idea is realized in [3] for the cubic Swift-Hohenberg equation under certain parameter regions.

In Section 3.1, we briefly review the topological verification method. Let us note that localized patterns require many modes to be approximated by Fourier expansion and that the equation (1) has the quintic nonlinearity. These facts cause huge computational cost for the verification, especially for estimates of nonlinear parts. Therefore in Section 3.2, we propose an improvement to efficiently obtain the estimates of the nonlinear terms. A key idea comes from the pseudo-spectral method [13] and we explain that the computational cost for the nonlinear terms may be suppressed by using a Fast Fourier Transform (FFT). Several rigorous numerical results of the existence of localized patterns on snaky branches are shown in Section 3.3.

The method we used here may be regarded as one of the tools to prove the numerically obtained continuation branch. However, we can not prove the existence of the whole snaky branch at present, therefore we need another improvement to reduce the computational cost. We conclude this paper with the discussion about the relationship between the computational difficulty to verify the whole snaky branch and behaviors of critical eigenvalues along this branch in Section 4.

2. Bifurcation Structures

2.1. Weak nonlinear analysis

Let us consider local bifurcation structures by the weak nonlinear analysis, *i.e.* the center manifold reduction. First of all, let us assume that $u \in L^2_{loc}$ is an L_0-periodic function and let a fundamental wave number be denoted by $k_0 = 2\pi/L_0$. We denote $\|u\|_{L^2} = \|u\|_{L^2(0,L_0)}$. Then a dispersion relation for each mode j is given by $\zeta_j = \nu - (1 - j^2k_0^2)^2$. Hence, a set

$$C_j = \{(\nu, k_0) \mid \nu = \nu_j(k_0) = (1 - j^2k_0^2)^2\}$$

represents a neutral stability curve for each mode j (see Figure 1). Our interest in this section is to study rigorous bifurcation structures with the nonlinear terms.

It should be noted that three curves do not intersect each other except at $(\nu, k_0) = (1, 0)$. Therefore, at most two elements in the set $\{\zeta_j\}_{j\geq 0}$ are zero at the same parameter values. Remark that $\{\zeta_j\}$ is going to be a set of eigenvalues for the linearization of ODEs (2) below at the origin. Let us define $\nu_*(k_0) = \min_{j\in\mathbb{Z}} \nu_j(k_0)$. Then, we only have to study the following two special cases, since we are interested in the first instability:

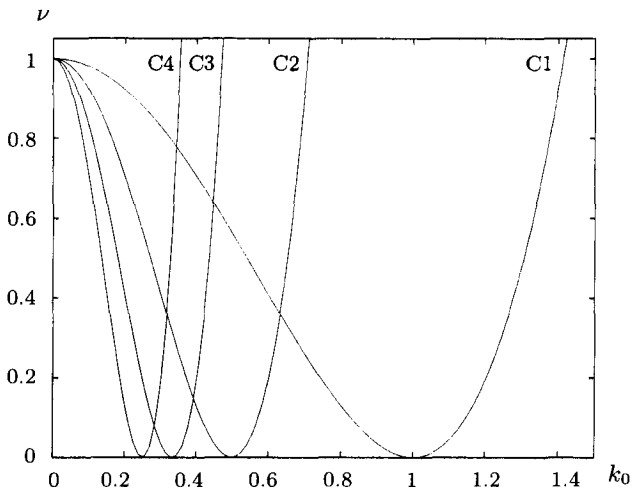

Fig. 1. Neutral stability curves for $j = 1, 2, 3, 4$.

1. (Simple critical point) There exists $n \geq 1$ such that if $\nu_*(k_0) = \nu_n(k_0)$ and $|j| \neq n$, then $\nu_*(k_0) < \nu_j(k_0)$.
2. (Double critical point) There exists $n \geq 1$ such that if $\nu_*(k_0) = \nu_n(k_0) = \nu_{n+1}(k_0)$ and $|j| \neq n, n+1$, then $\nu_*(k_0) < \nu_j(k_0)$.

Let us decompose $u(x,t)$ into a Fourier series

$$u(x,t) = \sum_{j \in \mathbb{Z}} \alpha_j(t) e^{ijk_0 x}, \quad \alpha_j(t) \in \mathbb{C}, \quad i = \sqrt{-1}.$$

This decomposition leads to the following system of ordinary differential equations

$$\dot{\alpha}_j = \zeta_j \alpha_j + \mu f_j^{(3)}(\alpha) - f_j^{(5)}(\alpha), \quad j \in \mathbb{Z}, \tag{2}$$

where

$$\zeta_j = \nu - \left(1 - j^2 k_0^2\right)^2, \quad f_j^{(3)}(\alpha) = \sum_{\substack{m_1+m_2+m_3=j \\ m_i \in \mathbb{Z}}} \alpha_{m_1} \alpha_{m_2} \alpha_{m_3}$$

and

$$f_j^{(5)}(\alpha) = \sum_{\substack{m_1+m_2+m_3+m_4+m_5=j \\ m_i \in \mathbb{Z}}} \alpha_{m_1} \alpha_{m_2} \alpha_{m_3} \alpha_{m_4} \alpha_{m_5}.$$

By the general theory [10] this system of ODEs is well-posed on the space:

$$X = \left\{ \alpha = (\alpha_j) \;\middle|\; \|\alpha\|_X^2 := \sum_{j \in \mathbb{Z}} |\alpha_j|^2 (1 + k_0^2 j^2)^4 < \infty \right\}.$$

First of all, we consider the simple critical case for the mode n. Then we have two critical modes which correspond to the center space $X_c = \mathrm{span}\{\alpha_n, \alpha_{-n}\}$. Let $X_s \subset X$ be a stable space which is spanned by all the other modes and $X = X_s \oplus X_c$. By the standard center manifold theory [16] we can construct a local invariant manifold $\mathcal{C}$ which is tangent to X_c at $\alpha = 0$ when $\zeta_n = \nu - \nu_n(k_0) = 0$. The center manifold is characterized locally by a graph of a smooth function $h\colon U \to X_s$ where $U \subset X_c \times \mathbb{R}$ is a neighborhood of $(\alpha, \zeta_n) = 0$ with $\|h(\alpha_c, \zeta_n)\|_X \le C(|\zeta_n| + \|\alpha_c\|_X)\|\alpha_c\|_X$. Here, $\alpha_c = (\alpha_n, \alpha_{-n})$ and C is a constant which is independent of (α_c, ζ_n). And the dynamics on the center manifold is obtained by just neglecting the effect from α_j with $|j| \neq n$ as

$$\dot{\alpha}_n = \zeta_n \alpha_n + 3\mu\alpha_n|\alpha_n|^2 - 10\alpha_n|\alpha_n|^4 + O(\delta^6), \tag{3}$$

since that effect produces only higher order terms of $|\alpha_n| = O(\delta)$ when $\zeta_n = O(\delta^4)$ and $\mu = O(\delta^2)$. Let us here introduce a polar coordinate $\alpha_n(t) = a_n(t)\exp(i\phi_n(t))$. Then the dynamics on the center manifold takes the following form

$$\dot{a}_n = \zeta_n a_n + 3\mu a_n^3 - 10a_n^5 + O(\delta^6) \tag{4}$$

$$\dot{\phi}_n = O(\delta^6). \tag{5}$$

As is easily observed, this system is structural unstable. To avoid this problem, we first restrict Fourier coefficients to real numbers. For the original variable $u(x,t)$, this restriction corresponds to even functions in L^2_{loc}. Since the quintic Swift-Hohenberg equation has a translation invariant property $u(x,t) \to u(x+\theta,t)$, the dynamics on the center manifold (3) can be recovered from the restricted problem. From this argument and the equation (4), we can conclude that a subcritical pitchfork bifurcation occurs around the simple critical point.

Next, let us study dynamics near a double critical point for the n, $n+1$ modes. As well as the simple critical point, the dynamics on the center manifold is governed by the following system

$$\begin{aligned}
\dot{\alpha}_n &= \zeta_n\alpha_n + 3\mu\alpha_n|\alpha_n|^2 + 6\mu\alpha_n|\alpha_{n+1}|^2 \\
&\quad - 10\alpha_n|\alpha_n|^4 - 60\alpha_n|\alpha_n|^2|\alpha_{n+1}|^2 - 30\alpha_n|\alpha_{n+1}|^4 + O(\delta^6), \\
\dot{\alpha}_{n+1} &= \zeta_{n+1}\alpha_{n+1} + 3\mu\alpha_{n+1}|\alpha_{n+1}|^2 + 6\mu\alpha_{n+1}|\alpha_n|^2 \\
&\quad - 10\alpha_{n+1}|\alpha_{n+1}|^4 - 60\alpha_{n+1}|\alpha_n|^2|\alpha_{n+1}|^2 - 30\alpha_{n+1}|\alpha_n|^4 + O(\delta^6).
\end{aligned}$$

In the following, we assume $u(\,\cdot\,,t)$ to be even functions. Then we obtain the following system

$$\begin{aligned}
\dot{a}_n &= a_n\left(\zeta_n + 3\mu a_n^2 + 6\mu a_{n+1}^2 - 10a_n^4 - 60a_n^2a_{n+1}^2 - 30a_{n+1}^4\right) + O(\delta^6), \\
\dot{a}_{n+1} &= a_{n+1}\left(\zeta_{n+1} + 3\mu a_{n+1}^2 + 6\mu a_n^2 - 10a_{n+1}^4 - 60a_n^2a_{n+1}^2 - 30a_n^4\right) + O(\delta^6).
\end{aligned} \tag{6}$$

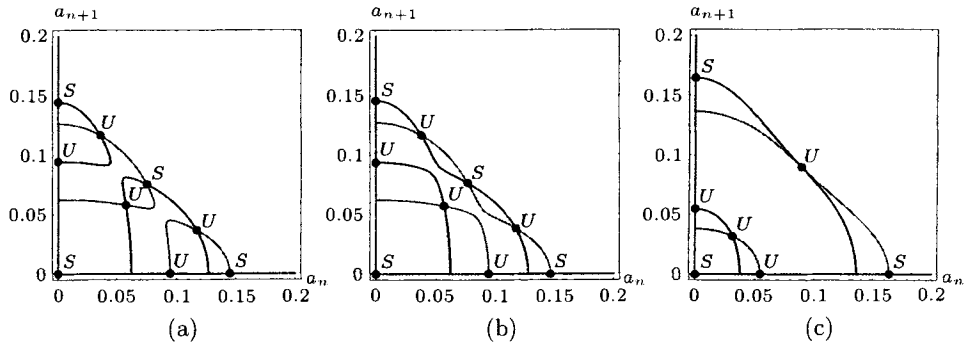

Fig. 2. Nullclines of (6) with $\mu = 0.1$ for (a) $p = -0.00189$ (b) $p = -0.00186$ (c) $p = -0.0008$. Gray lines and dark lines correspond to $\dot{a}_n = 0$ and $\dot{a}_{n+1} = 0$, respectively.

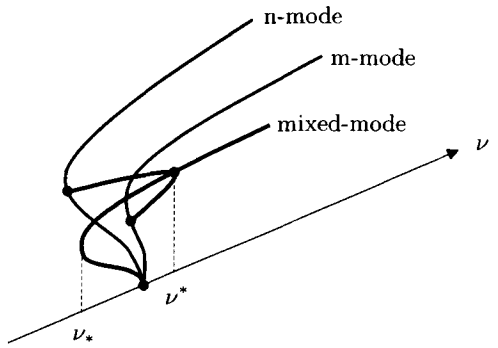

Fig. 3. Schematic bifurcation structure of pitchfork bifurcations.

Now let us first consider the case when $\zeta_n = \zeta_{n+1} = p$. Note that p differs from ν by a constant: $p = \zeta_n = \nu - (1 - n^2k_0^2)^2$. By a simple algebraic calculation we can conclude that we have a stable mixed mode solutions in a subcritical region $p \in (-81\mu^2/400, -9\mu^2/80)$ (see Figure 2). This stable mixed mode solution appears from a saddle-node bifurcation at $\nu = \nu_*$ which corresponds to $p = -81\mu^2/400$ and loses its stability by a subcritical pitchfork bifurcation at $\nu = \nu^*$, that is $p = -9\mu^2/80$ (see Figure 3). Bifurcation diagrams in the general case, $\zeta_n \neq \zeta_{n+1}$, are obtained by the imperfection of the pitchfork bifurcation. Two pictures in Figure 4 describe how this imperfection is observed in bifurcation diagrams. A parameter value for the left picture in Figure 4 is closer to the degenerate case $\zeta_n = \zeta_{n+1}$ than that for the right picture. Two branches of n and $n + 1$ mode solutions almost overlap each other in the left picture, while they are apart from each other in the right picture. Therefore the bifurcation diagram in the left picture is very close to the L^2 projection of Figure 3. Also at the degenerate case: $\zeta_n = \zeta_{n+1}$ two pure modes and mixed mode solutions appear as subcritical pitchfork bifurcations at the

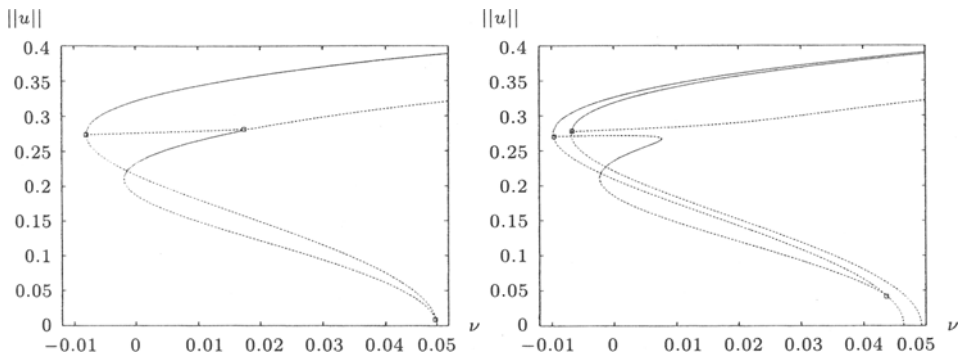

Fig. 4. Imperfection of pitchfork bifurcations ($\mu = 0.5$).

same value of ν coincidently (Figure 2 (c)). While, on the other hand, these three pitchfork bifurcations occur separately in general. Therefore in this weak nonlinear region we generically observe the "Z-shaped" branches for the mixed mode solutions which coincide with numerical global bifurcation diagrams in Figure 4 (derivations of these diagrams are treated in Section 2.2). Here we again assume that $\mu = O(\delta^2)$ since all of the fixed points we are interested in should be included in $\alpha_c = O(\delta)$.

2.2. Snaky structures and localized patterns

The results of the previous subsection provide us with the complete information concerning the local bifurcation structures around the trivial solution. It is, however, not enough to understand the whole bifurcation structure far away from the weak nonlinear region. To study the structure in these regions, numerical branch continuations by the pseudo-arclength method [8] to a Galerkin approximated problem:

$$\dot{a}_j = \zeta_j a_j + \mu \sum_{\substack{m_1+m_2+m_3=j \\ |m_i|\le m}} a_{m_1} a_{m_2} a_{m_3} - \sum_{\substack{m_1+m_2+m_3+m_4+m_5=j \\ |m_i|\le m}} a_{m_1} a_{m_2} a_{m_3} a_{m_4} a_{m_5}, \qquad j = 0, 1, \ldots, m \tag{7}$$

play a central role. Here $\{a_j\}$ are coefficients of the Fourier cosine expansion

$$u(x,t) = \sum_{|j|\le m} a_j(t) \cos(jk_0 x), \quad a_j(t) \in \mathbb{R}$$

with $a_{-j}(t) = a_j(t)$. Remark that we again restrict $u(\,\cdot\,, t)$ to even functions.

Let us fix the fundamental wave number $k_0 = 0.1$ and investigate bifurcation structures with different μ. Figure 5 expresses the bifurcation diagrams for equilibria of the equation (7) at $\mu = 0.5, 1.0, 1.5$, respectively. Here solid lines and dotted lines express stable and unstable branches, respectively. We easily observe that at each μ the first bifurcation branch arises as a subcritical pitchfork type. Moreover, the second bifurcation occurs from the first bifurcation branch. Numerical evidence shows that this new branch originates from one of the pieces of the

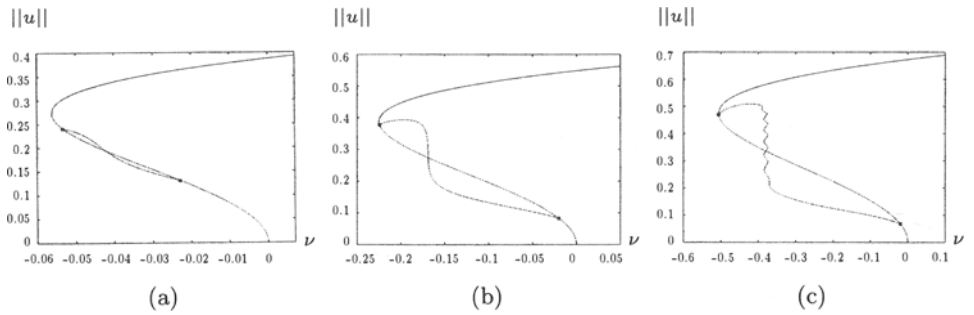

Fig. 5. Bifurcation diagrams at (a) $\mu = 0.5$ (b) $\mu = 1.0$ (c) $\mu = 1.5$ ($k_0 = 0.1$).

imperfected pitchfork bifurcation for the mixed mode. Notice that the branch of the mixed mode solutions become close to the "Z-shaped" branch if it is close to the degenerate case.

Moreover, if we increase the parameter μ further, we obtain a snaky bifurcation structure of saddle-node bifurcations (Figure 6). Let us denote each layer on the snaky branch by U_k and S_k as is described in the figure. The stationary solutions especially on lower layers have localized wave profile as are seen in Figure 7. These observations imply that the stable localized patterns appearing at the lower layers of the snaky structure correspond to those appearing in [14] by computer simulations. We remark that the number of the peaks of localized patterns increases as k becomes large. Due to the limitation of the system size L_0, these localized patterns change their shapes into that of the pure mode solution when the snaky branch approaches the bifurcation point at the original pure mode branch.

Furthermore, we numerically study the dynamics of solutions close to those

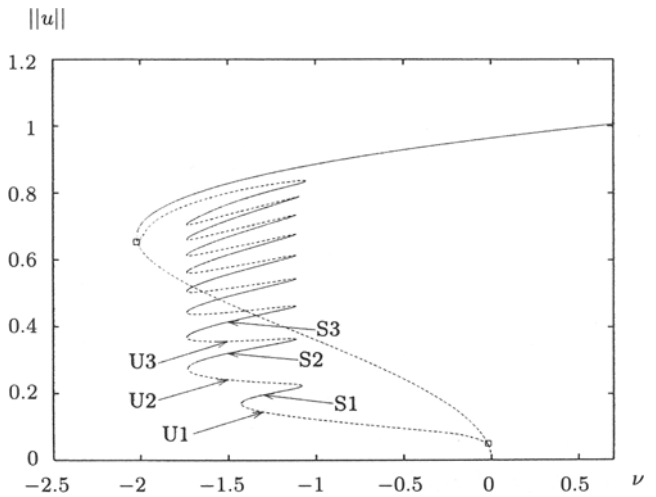

Fig. 6. Bifurcation diagram at $\mu = 3.0$ ($k_0 = 0.1$).

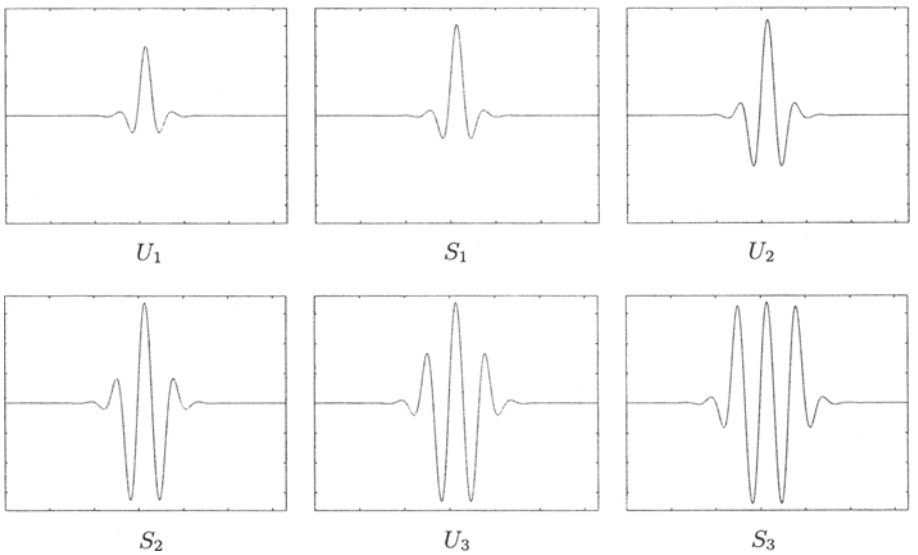

Fig. 7. Profiles of equilibria on the layers U_k, S_k, $k = 1, 2, 3$, ($\nu = -1.3$).

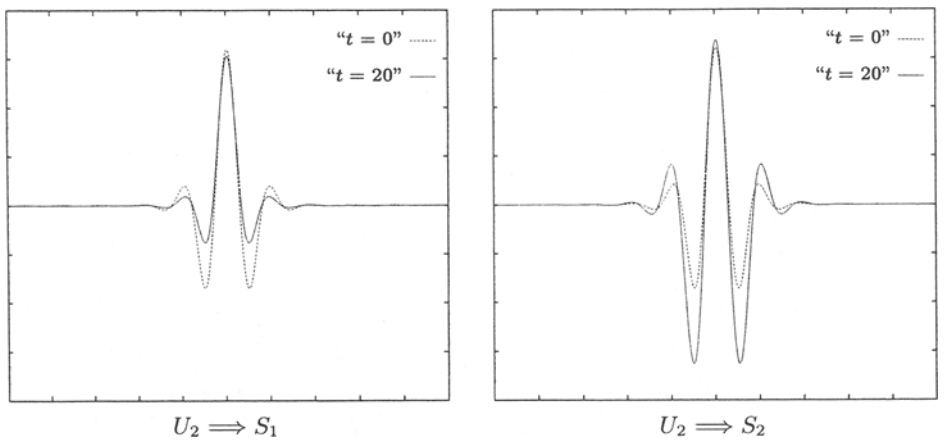

Fig. 8. Connection between unstable and stable equilibria ($\nu = -1.3$).

on the snaky branch. Two different time evolutions of almost same initial data on U_2-layer at $\nu = -1.3$ with small perturbations are shown in Figure 8. Each graph in Figure 9 describes the transition of L^2-norm corresponding to each time evolution in Figure 8. As is easily observed, depending on the small perturbations, unstable equilibrium point converges to stable equilibria on S_1-layer or S_2-layer. Therefore these numerical simulations imply that there exist connecting orbits from the stationary solution on U_2-layer to that on both S_1-layer and S_2-layer.

It should be mentioned that we can observe transient behavior so called

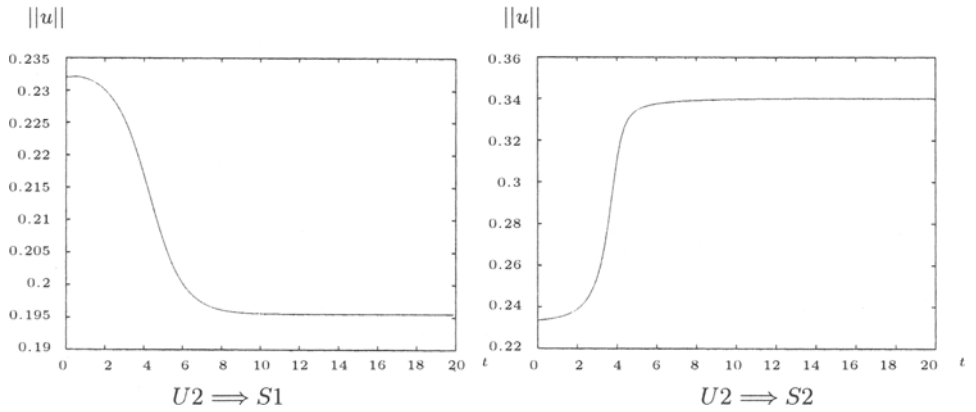

Fig. 9. Time evolution of L^2 norm ($\nu = -1.3$).

"aftereffects" of saddle-node bifurcations in [11]. More precisely, we can observe invading dynamics with the aftereffect of the hierarchical structure of saddle-node points by choosing the parameter ν carefully. Namely, when ν is slightly larger than the right saddle-node line, say $\nu = -1.1015$, the stable roll invades the stable uniform state temporally stagnating around each saddle-node bifurcation point. On the other hand, when ν is slightly smaller than the left saddle-node line, say $\nu = -1.7370$, the roll recedes from the uniform state, again temporally stagnating around each saddle-node point (Figure 10).

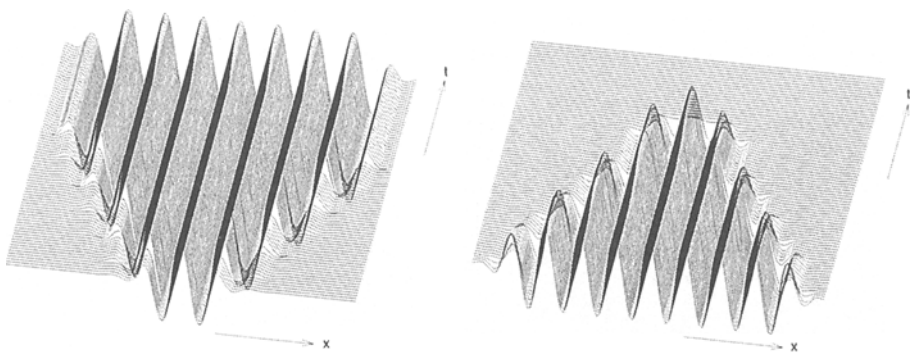

Fig. 10. Invading dynamics with the aftereffect of saddle-node points.

Although these phenomena studied in this subsection are derived from the finitely approximated problems, they imply the possibility of the rich dynamical structures for the quintic Swift-Hohenberg equation. Therefore, to clarify an essence of these phenomena, we need to investigate rigorously the existence of the localized solutions of the quintic Swift-Hohenberg equation and hopefully verify the snaky branch.

3. Rigorous Numerics

This section is devoted to the rigorous numerics in order to prove the existence of the localized patterns on the snaky branch. We briefly review the topological verification method with the Conley index theory in Section 3.1. In Section 3.2, we shall improve the method to efficiently obtain estimates of nonlinear terms, which are essential for the verification. This improvement is indispensable to apply the topological verification method to the localized patterns of the quintic Swift-Hohenberg equation. Finally in Section 3.3, we try to verify the existence of localized patterns observed in the preceding section.

3.1. Topological verification method

The Conley index plays an important role in the topological verification method. We first recall the elementary results of the Conley index theory (see [2, 15] for more detailed introductions).

Let $\varphi\colon \mathbb{R}\times X \to X$ be a flow on a locally compact metric space X. A compact set N is defined as an isolating neighborhood if the maximal invariant set $\mathrm{Inv}(\varphi, N)$ in N with respect to φ is contained in $\mathrm{Int}\, N$, the interior of N. That is $\mathrm{Inv}(\varphi, N) \subset \mathrm{Int}\, N$. This maximal invariant set is called the isolated invariant set. Moreover, the neighborhood N is defined as an isolating block, if the boundary of an isolating neighborhood ∂N consists of the union of

$$L^+ := \{x \in \partial N \mid \exists t > 0 \text{ s.t. } \varphi((0,t),x) \cap N = \emptyset\},$$
$$L^- := \{x \in \partial N \mid \exists t > 0 \text{ s.t. } \varphi((-t,0),x) \cap N = \emptyset\}.$$

L^+ and L^- are called the exit set and the entrance set of N, respectively.

DEFINITION 1. *The* Conley index *of the isolated invariant set* $\mathrm{Inv}(\varphi, N)$ *is defined by*

$$CH_*(\mathrm{Inv}(\varphi, N)) := H_*(N, L^+).$$

Here the notation $H_*(N, L^+)$ denotes the relative homology. We remark that the Conley index can also be defined by the homotopy class of the quotient space N/L^+. More precisely, let $N \supset L$ be a pair of topological spaces and $(N/L, [L]) := ((N \setminus L) \cup \{\dagger\}, \{\dagger\})$ denote a pointed topological space obtained by identifying the points in L to one point $\dagger$. Then the homotopy Conley index is also defined by the homotopy class of $(N/L^+, [L^+])$. By the basic homology theory, the previous definition of the Conley index is equivalent to the homology of $(N/L^+, [L^+])$, i.e. $H_*(N, L^+) = H_*(N/L^+, [L^+])$.

It should be noted that the above definition is well-defined [2, 15]. More precisely, we can check that there exists an isolating block for any given isolated invariant set. In addition, if (N_1, L_1^+) and (N_2, L_2^+) are pairs of isolating blocks and exit sets for the same isolated invariant set, then

$$CH_*(N_1, L_1^+) = CH_*(N_2, L_2^+).$$

Next, let us move on to the topological verification method. Recall that the quintic Swift-Hohenberg equation decomposed into Fourier cosine bases $u(x,t) = \sum_{j\in\mathbb{Z}} a_j(t)\cos(jk_0x)$ with $a_j = a_{-j}$ takes the following form

$$\dot{a}_j = f_j(a) = \zeta_j a_j + \mu f_j^{(3)}(a) - f_j^{(5)}(a), \quad j \in \mathbb{Z}, \tag{8}$$

where

$$f_j^{(3)}(a) = \sum_{\substack{m_1+m_2+m_3=j \\ m_i\in\mathbb{Z}}} a_{m_1}a_{m_2}a_{m_3}$$

and

$$f_j^{(5)}(a) = \sum_{\substack{m_1+m_2+m_3+m_4+m_5=j \\ m_i\in\mathbb{Z}}} a_{m_1}a_{m_2}a_{m_3}a_{m_4}a_{m_5}$$

with $a = (a_0, a_1, \ldots)$. Since we can treat only finite dimensional problems numerically, it is convenient to adopt the following decomposition

$$\dot{a}_F := f_F(a_F, a_I) = (f_0(a), f_1(a), \ldots, f_m(a)),$$
$$\dot{a}_I := f_I(a_F, a_I) = (f_{m+1}(a), f_{m+2}(a), \ldots),$$

where $a_F := (a_0, a_1, \ldots, a_m)$ and $a_I := (a_{m+1}, a_{m+2}, \ldots)$. We remark that in the rest of this paper the subscript F and I means finite part and infinite part separated by a prescribed integer $m \geq 0$, respectively.

Let us define the projection $P_j\colon (a_0, a_1, \ldots) \mapsto a_j$ for each j.

DEFINITION 2 ([3]). *A compact set $W = \prod_{j\geq 0}[a_j^-, a_j^+]$ is called a* lifting set *with respect to* (8), *if there exists an integer $m \geq 0$ such that the followings hold*:

1. *There exists a compact set $N \subset W_F = \prod_{0\leq j\leq m}[a_j^-, a_j^+]$ and, $N \times W_I$, where $W_I = \prod_{j>m}[a_j^-, a_j^+]$, forms a self-consistent a priori bound* [19].
2. *N is an isolating block for the flow $\varphi^{(a_I)}$ induced by the vector field $f_F(a_F, a_I)$ for each $a_I \in W_I$.*
3. *For $j > m$,*

$$P_j(f(a)) < 0, \quad \text{for } P_j(a)|_{a_F\in N} = a_j^+,$$
$$P_j(f(a)) > 0, \quad \text{for } P_j(a)|_{a_F\in N} = a_j^-.$$

We are now ready to show the important theorem which plays a central role in the topological verification method.

THEOREM 3 ([19]). *Let W be a lifting set and $N \subset W_F$ be a compact set corresponding to that in the condition* 1 *of Definition* 2. *If the Conley index of the isolating block N takes*

$$CH_i(\mathrm{Inv}(\varphi^{(a_I)}, N)) \cong \begin{cases} \mathbb{Z}, & i = n, \\ 0, & \text{otherwise} \end{cases}$$

for some $n \in \{0, 1, \ldots, m\}$, *then there exists an equilibrium point for* (8) *in* $N \times W_I$.

Let $\overline{a} = (\overline{a}_F, 0)$ be an approximate equilibrium obtained by the Galerkin approximated finite dimensional system, like an equilibrium corresponding to a localized pattern in the previous section. The lifting set W is supposed to include the approximate equilibrium point $\overline{a}$ for the verification. To verify the above conditions for the lifting set by rigorous numerics, we assume a power decay property on the infinite part, *i.e.*

$$W_I = \prod_{j>m} \left[-\frac{c}{j^s}, \frac{c}{j^s}\right] \tag{9}$$

for a positive constant c and an integer $s \geq 2$.

In order to construct an isolating block N and to check the inwardness of the vector fields on the boundary $N \times \partial W_I$, it is convenient to introduce a new variable $x = (x_F, x_I)$ satisfying

$$(Px_F + \overline{a}_F, x_I) = (a_F, a_I), \quad P = [p_0 p_1 \cdots p_m],$$

where p_j is an eigenvector of the Jacobi matrix of $f_F(a_F, a_I)$ around $\overline{a}$. Let us denote this transformation by $T\colon x = (x_F, x_I) \mapsto (Px_F + \overline{a}_F, x_I)$. Then the system on the x-coordinate is expressed by

$$\dot{x}_j = \lambda_j x_j + \epsilon_j(Tx), \quad j = 0, 1, \ldots,$$

where λ_j is an eigenvalue associated with the eigenvector p_j for $0 \leq j \leq m$ and is ζ_j for $j > m$ from the property of the transformation. Note that $\epsilon_j(Tx)$ is the higher order error term, whose absolute value is expected to be smaller than that of the linear part.

We check the conditions on Theorem 3 on this system. More precisely, we first prepare on the x-coordinate

$$\widetilde{W} = \widetilde{W}_F \times \widetilde{W}_I, \quad \widetilde{W}_F = \prod_{0 \leq j \leq m} [x_j^-, x_j^+], \quad \widetilde{W}_I = \prod_{j>m} \left[-\frac{c}{j^s}, \frac{c}{j^s}\right]$$

with $0 \in \widetilde{W}$ such that $T_F(\widetilde{W}_F) \subset W_F$. Then we construct an isolating block in $\widetilde{W}_F$ and check the inwardness of the vector field on the boundary $\widetilde{W}_F \times \partial \widetilde{W}_I$ by obtaining the estimate $I_j(\widetilde{W})$ as an interval such that

$$\epsilon_j(Tx) \in I_j(\widetilde{W}) \text{ for } x \in \widetilde{W}.$$

In the real computations, since we can derive the explicit form of $\epsilon_j(a)$ expressed by the a-coordinate, we make use of an other interval $I_j(W)$ for the estimate such that

$$\epsilon_j(a) \in I_j(W) \text{ for } a \in W. \tag{10}$$

Note that $I_j(\widetilde{W}) \subset I_j(W)$. As is clearly observed, the transversarity of the vector field on the boundary may be easily checked on computers in the x-coordinate rather than in the a-coordinate. We refer [3, 6, 19] for the details of the algorithm of the topological verification method.

3.2. Estimates of nonlinear terms

One of the essences of the topological verification method is to make use of the hyperbolicity of the equilibrium point to construct a desirable lifting set. Precisely, the hyperbolicity of the linear part is needed to suppress the nonlinear error part $\epsilon_j(a)$. Therefore, we have much more opportunity to succeed in the verification if we could have efficient estimates of $I_j(W)$.

Let us consider the following summation, which is a generalized form for a j-th Fourier mode of a p-th nonlinear term.

$$\sum_{\substack{m_1+m_2+\cdots+m_p=j \\ m_i\in\mathbb{Z}}} a_{m_1}a_{m_2}\cdots a_{m_p}, \quad j \in \mathbb{Z}. \tag{11}$$

Recall that, from the arguments in [3, 4, 6, 19], the explicit expressions of $I_j(W)$ consist of the union of the above summation (11). Moreover, due to the power decay property (9) of the infinite part, the analytical estimates can be derived for the case of $\max(|m_i|) > m$ or $j > m$. On the other hand, the collection of the finite sums

$$\sum_{\substack{m_1+m_2+\cdots+m_p=j \\ |m_i|\le m}} a_{m_1}a_{m_2}\cdots a_{m_p}, \quad j = 0, 1, \ldots, m \tag{12}$$

should be calculated on computers with interval arithmetic. If we directly calculate this collection, it requires $O(m^p)$ computational costs. As is observed in Section 2.2, localized patterns require much more modes to be approximated by the Fourier expansion compared to simple mixed mode patterns. It means that the number m, which separates the finite part and the infinite part, should be large. Therefore the computational cost of the direct calculation performed as before in [3, 4, 6, 19] for (12) grows proportionally to m^p. The purpose of this subsection is to present an improvement to efficiently calculate the finite sum (12). The key idea comes from the pseudo-spectral method, which is well-known as one of the computer simulation methods.

Let us first treat the quadratic case ($p = 2$) for the sake of simplicity. Consider the discrete Fourier transform and its inverse:

$$a_l = \mathcal{F}(u)|_l = \sum_{j=0}^{2m-1} u(x_j)e^{-ilk_0x_j}, \tag{13}$$

$$u(x_j) = \mathcal{F}^{-1}(a)|_j = \frac{1}{2m}\sum_{l=-m+1}^{m} a_l e^{ilk_0x_j}, \tag{14}$$

whose size are $2m$. Here $\left\{x_j = \frac{L_0}{2m} j\right\}$, $j = 0, 1, \ldots, 2m-1$, are grid points in the interval $[0, L_0]$.

The basic idea of the pseudo-spectral method is the following. First of all, we pull back the Fourier coefficients $\{a_l\}$ to the original physical variable $\{u(x_j)\}$ by (14). Then we calculate the nonlinear term $\{u^2(x_j)\}$ at each point. Finally, the summation (12) may be calculated by transforming $\{u^2(x_j)\}$ to each Fourier element by (13). These arguments can be described as follows,

$$\begin{aligned} c_l &= \sum_{j=0}^{2m-1} u(x_j)^2 e^{-ilk_0 x_j} \\ &= \frac{1}{(2m)^2} \sum_{j=0}^{2m-1} \left(\sum_{m_1=-m+1}^{m} a_{m_1} e^{im_1 k_0 x_j} \right) \left(\sum_{m_2=-m+1}^{m} a_{m_2} e^{im_2 k_0 x_j} \right) e^{-ilk_0 x_j} \\ &= \frac{1}{2m} \sum_{\substack{m_1+m_2=l \\ -m+1 \le m_i \le m}} a_{m_1} a_{m_2} + \frac{1}{2m} \sum_{\substack{m_1+m_2=l\pm 2m \\ -m+1 \le m_i \le m}} a_{m_1} a_{m_2}. \end{aligned} \tag{15}$$

Recall that the second term of (15) is called an aliasing error. This error is incorporated to the convolution because two different Fourier modes by modulo $2m$ can not be distinguished due to discretization. One of the popular methods to remove aliasing errors is as follows ([13]). Extend the size of the discrete Fourier transform from $2m$ to $2m\delta$ for $\delta > 1$ and let $\{a_j\}$ be

$$\begin{cases} a_j = 0, & \text{for } m+1 \le j \le \delta m \text{ and } -\delta m + 1 \le j \le -m-1, \\ a_{-m} = a_m. \end{cases}$$

Then, the same calculation as above for extended Fourier coefficients leads to

$$\begin{aligned} \hat{c}_l &= \sum_{j=0}^{2\delta m-1} u(x_j)^2 e^{-ilk_0 x_j} \\ &= \frac{1}{2\delta m} \sum_{\substack{m_1+m_2=l \\ |m_i| \le m}} a_{m_1} a_{m_2} + \frac{1}{2\delta m} \sum_{\substack{m_1+m_2=l\pm 2\delta m \\ |m_i| \le m}} a_{m_1} a_{m_2}. \end{aligned} \tag{16}$$

Hence if $\delta > \frac{3}{2}$, then second term which causes the aliasing error can be eliminated and the finite summation (12) for $p = 2$ is calculated by

$$\sum_{\substack{m_1+m_2=l \\ |m_i| \le m}} a_{m_1} a_{m_2} = 2m\delta \hat{c}_l.$$

The same approach can be applied to the general nonlinear term (12) by taking δ suitably. Note that by using FFT implemented with interval arithmetic we obtain the rigorous bounds of (12) quite efficiently.

For the quintic Swift-Hohenberg equation, $p = 3$ and $p = 5$ are important cases and the following lemma may be obtained easily.

LEMMA 4. *A sufficient condition to remove aliasing errors is* $\delta > 2$ *for* $p = 3$ *and* $\delta > 3$ *for* $p = 5$, *respectively.*

3.3. Existence of localized patterns

Let us denote the stationary solution corresponding to the equilibrium on the lower layers of the snaky branch in Figure 6 by

$$u(x; k_0, \nu, b) = \sum_{|j| \le m} a_j \cos(j k_0 x),$$

where the set of the Fourier coefficients $\{a_j\}$ corresponds to the approximated equilibrium on each layer $b = U_k, S_k$, $k = 1, 2, 3$, at the parameter value ν.

Then, we obtain the following theorems by the topological verification method.

THEOREM 5. *Let* $\nu = -1.3$, $k_0 = 0.1$ *and* $\mu = 3.0$. *Then, at each point* $u(x; k_0, \nu, b)$, $b = U_k, S_k$, $k = 1, 2, 3$, *there exists a stationary solution* $u_*(x; k_0, \nu, b)$ *of the quintic Swift-Hohenberg equation such that*

$$\begin{aligned}
&\|u_*(x; k_0, \nu, U_1) - u(x; k_0, \nu, U_1)\|_{L^2} \le 1.04077019 \times 10^{-8} \\
&\|u_*(x; k_0, \nu, S_1) - u(x; k_0, \nu, S_1)\|_{L^2} \le 1.57739803 \times 10^{-8} \\
&\|u_*(x; k_0, \nu, U_2) - u(x; k_0, \nu, U_2)\|_{L^2} \le 2.44819377 \times 10^{-8} \\
&\|u_*(x; k_0, \nu, S_2) - u(x; k_0, \nu, S_2)\|_{L^2} \le 4.31155312 \times 10^{-8} \\
&\|u_*(x; k_0, \nu, U_3) - u(x; k_0, \nu, U_3)\|_{L^2} \le 2.83246161 \times 10^{-9} \\
&\|u_*(x; k_0, \nu, S_3) - u(x; k_0, \nu, S_3)\|_{L^2} \le 7.47772691 \times 10^{-9}.
\end{aligned}$$

THEOREM 6. *Let* $\nu = -1.5$, $k_0 = 0.1$ *and* $\mu = 3.0$. *Then, at each point* $u(x; k_0, \nu, b)$, $b = U_k, S_k$, $k = 2, 3$, *there exists a stationary solution* $u_*(x; k_0, \nu, b)$ *of the quintic Swift-Hohenberg equation such that*

$$\begin{aligned}
&\|u_*(x; k_0, \nu, U_2) - u(x; k_0, \nu, U_2)\|_{L^2} \le 4.47782900 \times 10^{-8} \\
&\|u_*(x; k_0, \nu, S_2) - u(x; k_0, \nu, S_2)\|_{L^2} \le 4.57533187 \times 10^{-8} \\
&\|u_*(x; k_0, \nu, U_3) - u(x; k_0, \nu, U_3)\|_{L^2} \le 4.20841075 \times 10^{-8} \\
&\|u_*(x; k_0, \nu, S_3) - u(x; k_0, \nu, S_3)\|_{L^2} \le 6.82912523 \times 10^{-9}.
\end{aligned}$$

Here, the norm of the difference between a stationary solution and the approximate solution in the above theorems is estimated by the L^2-volume of each lifting set. It should be remarked that we set the power decay property (9) as $c = 1.0$ and $s = 5$ for all the verifications of the above theorems. Moreover, the dimension for the finite part is chosen as $m = 256$ for U_k, S_k, $k = 1, 2$, and $m = 512$ for U_3, S_3 in Theorem 5. In Theorem 6, $m = 256$ for U_2, S_2, U_3 and $m = 512$ for S_3. From these theorems, we can conclude that close to the localized patterns observed on the snaky branch in Figure 6 there really exists the stationary solution to the quintic Swift-Hohenberg equation (8), *i.e.* the original infinite dimensional problem.

4. Discussion

Throughout the present paper, we only studied periodic stationary solutions of the quintic Swift-Hohenberg equation. Therefore it should be mentioned here why we call the stationary solutions on the lower snaky branch "localized patterns." This is based on the following two observations: (i) Stationary solutions on the snaky branch can be numerically traced as k_0 varies. They persist no matter how large the period $L = 2\pi/k_0$ is. (ii) Although these continuations can be done up to certain numerical resolution, these stationary solutions can be expected to converge to homoclinic solutions (see [18], where they also found snaky branches of homoclinic solutions). In fact, if we draw the corresponding numerical orbits in the phase space of $(u, u_x, u_{xx}, u_{xxx})$ for several different parameter values of k_0, they seem to converge to a closed Jordan curve which passes the origin as $k_0 \to 0$. (see Figure 11.)

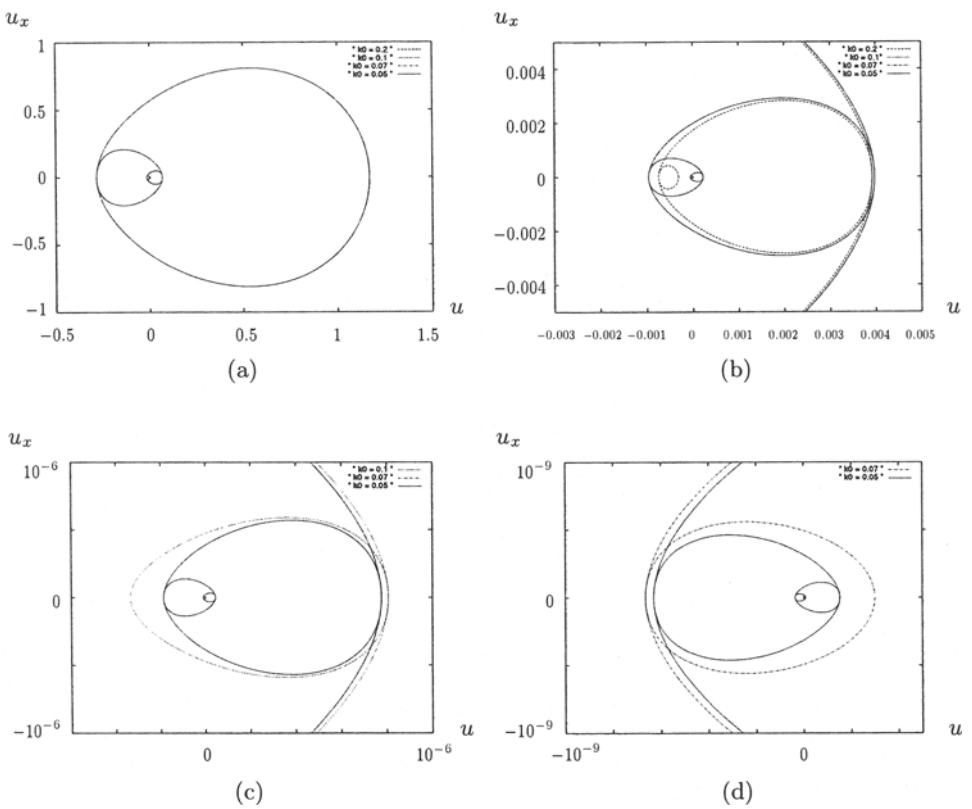

Fig. 11. (u, u_x)-projections of numerical periodic orbits on U_1-layers ($\nu = -1.3$, $\mu = 3.0$,) for $k_0 = 0.2, 0.1, 0.07, 0.05$, respectively. As expanding the neighborhood of origin ((a)→(b)→(c)→(d)), these orbits become distinguishable in order of thier periods.

All computations shown in the present paper is performed by 3 GHz Pentium 4 processor and gcc-3.2 compiler on RedHat 8.0 with the interval arithmetic software C-XSC [9]. As is mentioned in Section 1, our main purpose is to study the localized patterns on the snaky bifurcation branches, and we succeeded in proving the existence of several localized solutions (Theorem 5 and 6). However, the computation to verify the solutions on higher layers becomes more difficult rather than those on lower layers.

Recall that the crucial point of the topological verification method is to exploit the hyperbolicity of the equilibrium point to suppress the effects of the higher order error terms. On the other hand we can numerically check that the higher we go up the snaky branch, the more critical eigenvalues appear. Moreover, the distance between the most critical eigenvalue and the origin becomes much smaller on the higher layers than lower layers.

These properties of critical eigenvalues make it difficult to construct an isolating block by using the hyperbolicity around the equilibrium point on the higher layers of the snaky branch. To suppress the nonlinear error terms of the equilibria on these higher layers, it is inevitable to increase m, since their finite part dynamics possess weak hyperbolicity. Note that, FFT based algorithm to estimate nonlinear terms also works well for $m > 512$. However, we observe that the computational cost for several other parts in the algorithm of the topological verification method becomes large as m increases. For example, for the coordinate change from the a-coordinate to the x-coordinate, we need to solve an $m + 1$ dimensional linear equation. The algorithm we exploited to solve linear equations is based on the idea in [12], and it requires $\frac{2}{3}m^3$ computational costs. In fact, on the layer next to that we can prove, the necessary dimension for the finite part should be $m > 512$ and therefore the verifications are not performed in reasonable computational time.

Acknowledgments. The authors would like to express their sincere gratitude to Konstantin Mischaikow, Sarah Day, and Ciprian D. Coman for useful comments. This work is partially supported by the Ministry of Education, Science, Sports and Culture, Grant-in-Aid for J.S.P.S. Japan-US cooperative science program. The first author is partially supported by Grant-in-Aid for J.S.P.S. Fellows, 03948.

References

[1] C.J. Budd, G.W. Hunt and R. Kuske, Asymptotics of cellular buckling close to the Maxwell load. Proc. R. Soc. Lond. A, **457** (2001), 2935.

[2] C. Conley, Isolated Invariant Sets and the Morse Index. CBMS Lecture Notes **38**, A.M.S. Providence, R.I. 1978.

[3] S. Day, Y. Hiraoka, K. Mischaikow and T. Ogawa, Rigorous numerics for global dynamics: a study of the Swift-Hohenberg equation. Submitted.

[4] S. Day, O. Junge and K. Mischaikow, A rigorous numerical method for the global analysis of infinite dimensional discrete dynamical systems. In preparation.

[5] L.Yu. Glebsky and L.M. Lerman, On small stationary localized solutions for the generalized 1-D Swift-Hohenberg equation. Chaos, **5** (1995), 424.

[6] Y. Hiraoka, T. Ogawa and K. Mischaikow, Conley index based numerical verification method for global bifurcations of the stationary solutions to the Swift-Hohenberg equation. Trans.

Japan Soc. Indust. Appl. Math., **13**, No.2 (2003) 191.
[7] G. Iooss and M.C. Pérouéme, Perturbed homoclinic solutions in reversible 1:1 resonance vector fields. J. Diff. Eq., **102** (1993), 62.
[8] H.B. Keller, Lectures on Numerical Methods in Bifurcation Problems. Springer-Verlag. Notes by A.K. Nandakumaran and Mythily Ramaswamy, Indian Institute of Science, Bangalore. 1987.
[9] R. Klatte, U. Kulisch, A. Wiethoff, C. Lawo and M. Rauch, C-XSC: A C++ Class Library for Extended Scientific Computing. Springer-Verlag, 1993.
[10] A. Mielke and G. Schneider, Attractors for modulation equations on unbounded domains—existence and comparison. Nonlinearity, **8** (1995), 743.
[11] Y. Nishiura, Far-from-Equilibrium Dynamics. AMS Translations of Mathematical Monographs **209**, 2002.
[12] S. Oishi and M. Rump, Fast verification of solutions of matrix equations. Numer. Math., **90** (2002), 755.
[13] S. Orszag, Numerical simulation of incompressible flows within simple boundaries. I. Galerkin (spectral) representations. Stud. Appl. Math., **50** (1971), 293.
[14] H. Sakaguchi and H.R. Brand, Stable localized solutions of arbitrary length for the quintic Swift-Hohenberg equation. Physica D, **97** (1996), 274.
[15] D. Salamon, Connected simple systems and the Conley index of isolated invariant sets. Trans. Amer. Math. Soc., **291** (1985), 1.
[16] A. Vanderbauwhede and G. Iooss, Center manifold theory in infinite dimensions. Dynamics Reported **125**, Springer-Verlag, 1992.
[17] M.K. Wadee, C.D. Coman and A.P. Bassom, Solitary wave interaction phenomena in a strut buckling model incorporating restabilisation. Physica D, **163** (2002), 26.
[18] P.D. Woods and A.R. Champneys, Heteroclinic tangles and homoclinic snaking in the unfolding of a degenerate reversible Hamiltonian-Hopf bifurcation. Physica D, **129** (1999), 147.
[19] P. Zgliczyński and K. Mischaikow, Rigorous numerics for partial differential equations: The Kuramoto-Sivashinsky equation. Found. Comput. Math., **1** (2001), 255.